Environmental Pollution 253 (2019) 1089–1099

Contents lists available at ScienceDirect

Environmental Pollution

journal homepage: www.elsevier.com/locate/envpol

$PM_{2.5}$ elements at an urban site in Yangtze River Delta, China: High time-resolved measurement and the application in source apportionment☆

Yiyong Yu [a], Shuyan He [a], Xilan Wu [c], Chi Zhang [c], Ying Yao [c], Hong Liao [b], Qin'geng Wang [a, b, **], Mingjie Xie [b, *]

[a] State Key Laboratory of Pollution Control and Resources Reuse, School of the Environment, Nanjing University, Nanjing 210023, China
[b] Collaborative Innovation Center of Atmospheric Environment and Equipment Technology, Jiangsu Key Laboratory of Atmospheric Environment Monitoring and Pollution Control, School of Environmental Science and Engineering, Nanjing University of Information Science & Technology, 219 Ningliu Road, Nanjing 210044, China
[c] NUIST Reading Academy, Nanjing University of Information Science & Technology, 219 Ningliu Road, Nanjing 210044, China

ARTICLE INFO

Article history:
Received 17 January 2019
Received in revised form
9 June 2019
Accepted 18 July 2019
Available online 19 July 2019

Keywords:
$PM_{2.5}$
Elements
High time-resolved
Positive matrix factorization
Source apportionment

ABSTRACT

Elemental concentrations of ambient aerosols are commonly sampled over 12–24 h, and the low time resolution puts a great limit on current understanding about the temporal variations and source apportionment based on receptor models. In this work, hourly-resolved concentrations of eighteen elements in $PM_{2.5}$ at an urban site in Nanjing, a megacity in Yangtze River Delta of east China, were obtained by using a Xact 625 ambient metals monitor from 12/12/2016 to 12/31/2017. The influence of traffic activities was clearly reflected by the spikes of crustal elements (e.g., Fe, Ca, and Si) in the morning rush hour, and the firework burning and sandstorm events during the sampling periods were tracked by sharp enrichment of Ba, K and Fe, Ca, Si, Ti in $PM_{2.5}$, respectively. To evaluate the advantage of hourly-resolved elements data in identifying impacts from specific emission sources, positive matrix factorization (PMF) analysis was performed with the 1-h data set ($PMF_{1\text{-}h}$) and 23-h averaged data ($PMF_{23\text{-}h}$), respectively. The 4- and 6-factor $PMF_{23\text{-}h}$ solutions had similar factor profiles and consistent factor contributions as the corresponding $PMF_{1\text{-}h}$ solutions. However, due to the limit in inter-sample variability, PMF analysis with 23-h average data misclassified some major (e.g., K, Fe, Zn, Ca, and Si) and trace (e.g., Pb) elements in factor profiles, resulting in different absolute factor contributions between $PMF_{23\text{-}h}$ and $PMF_{1\text{-}h}$ solutions. These results suggested the use of high time-resolved data to obtain valid and robust source apportionment results.

1. Introduction

Particulate matter (PM) with aerodynamic diameter less than 2.5 μm ($PM_{2.5}$) is a complex mixture of chemicals often emitted from biomass burning, fossil fuel combustion, industrial processes, and atmospheric transformation of gaseous species. Both short- and long-term exposures to $PM_{2.5}$ are related to increased risk of mortality, as well as diseases of the respiratory and cardiac systems (Dockery et al., 1993; Pope et al., 2002; Pope and Dockery, 2006; Zanobetti and Schwartz, 2009). To examine the health effect of distinct $PM_{2.5}$ sources, compositional data were widely used as input for receptor modeling to retrieve $PM_{2.5}$ source contributions (Laden et al., 2000; Ito et al., 2006; Stanek et al., 2011; Bell et al., 2014). Ito et al. (2006) found some evidence of positive association of respiratory disease emergency department visits with $PM_{2.5}$ contributions from biomass burning in four U.S. cities; $PM_{2.5}$ road dust contributions were associated with cardiovascular hospitalizations in four counties in Connecticut and Massachusetts (USA) for persons ≥ 65 years of age. As such, identifying and quantifying $PM_{2.5}$ sources that are responsible for health effects is valuable in developing effective regulatory strategies to control specific sources.

☆ This paper has been recommended for acceptance by Dr. Haidong Kan.

* Corresponding author. 219 Ningliu Road, Nanjing, Jiangsu, 210044, China.
** Corresponding author. 163 Xianlin Ave., Nanjing, Jiangsu, 210023, China.
E-mail addresses: wangqg@nju.edu.cn (Q. Wang), mingjie.xie@nuist.edu.cn, mingjie.xie@colorado.edu (M. Xie).

https://doi.org/10.1016/j.envpol.2019.07.096
0269-7491/

Trace elements comprise a minor fraction (~10%) of ambient $PM_{2.5}$ (Marcazzan et al., 2001; Chang et al., 2018), far less than inorganic ions (e.g., SO_4^{2-}, NO_3^-, NH_4^+) and carbonaceous components (e.g., organic carbon). A number of studies reported that trace elements could serve as potential contributors to $PM_{2.5}$ toxicity (Pope et al., 2002; Li et al., 2010; Cho et al., 2012; Bell et al., 2014), and the trace elements are useful markers in resolving $PM_{2.5}$ source contributions, especially for dust related to traffic, crustal weathering and industrial processes, and/or soil resuspension (Xie et al., 2012; Dall'Osto et al., 2013; Chang et al., 2018; Wang et al., 2018). The elemental data used in most previous aerosol source apportionment studies were 24-h average concentrations (Kim et al., 2005a; Kim et al., 2005b; Qin et al., 2006; Kong et al., 2015). The limitation in time resolution might lead to the failure in identifying sources varying at different hours of the day. Wang et al. (2018) compared the source apportionment results of trace elements in $PM_{2.5}$ derived from hourly, 4- and 6-h averaged data. The results indicate that using hourly data will lead to more robust source apportionment than using data with lower time-resolution. Because the measurement data with high time-resolution (e.g., 1-h) have greater inter-sample variability than those integrated over long time periods (e.g., 24-h) (Dall'Osto et al., 2013). This is particularly important in resolving local aerosol sources (e.g, traffic) with peak contributions lasting for only a short time (e.g., 1–3 h).

Nanjing (118°22′ and 119°14′E, 31°14′ and 32°37′N), a typical mega-city located in Yangtze River Delta of east China with a population of over 6 million, is one of the fastest growing cities in China. The industries in Nanjing with substantial PM emissions include but not limited to petrochemicals, electronics, automobile, iron and steel, and thermal power. In this study, a Xact 625 ambient metals monitor (Cooper Environmental Services, OR, USA) was deployed at an urban site in Nanjing, China. Hourly concentrations of 23 elements in $PM_{2.5}$ were recorded for around one year, and the data set was prescreened and used for source apportionment with positive matrix factorization (PMF). No previous study measured $PM_{2.5}$ elements at 1-h resolution in urban area of Nanjing city, and two pollution episodes were captured during the measurement campaign with sharp increase in distinct mixtures of $PM_{2.5}$ elements. The one-year hourly resolved data (1-h data set) ensure representative observations of diurnal variations of $PM_{2.5}$ elements, and robust PMF source/factor profiles and contributions. In addition, the 23-h averages (1:00–24:00 for each day) of elements concentrations were calculated to simulate daily filter sampling and generate a new data set (23-h data set) for PMF analysis.

A number of previous studies performed hourly measurements of trace elements in $PM_{2.5}$ followed by source apportionment with receptor modeling (Dall'Osto et al., 2013; Park et al., 2014; Phillips-Smith et al., 2017; Chang et al., 2018; Wang et al., 2018). However, due to the lack of long-term hourly measurements, very few of them evaluated the advantage of using 1-h data for source apportionment compared to using daily average data. The primary goals of this work are to (1) characterize the high time-resolved variations of $PM_{2.5}$ elements in urban Nanjing, (2) retrieve distinct element sources using the 1-h data set from PMF analysis, and (3) illustrate the advantage of using high time-resolved data for source apportionment through the comparison of PMF results derived from 1-h and 23-h data sets.

2. Methods

2.1. Sampling site characteristics

The hourly measurements of $PM_{2.5}$ elements were performed on the rooftop of Nanjing Environmental Protection Building (NEPB, 118.75°E, 32.06°N), a six-storey building located in the downtown area of Nanjing city, China (Fig. S1, supplementary information). The NEPB site is surrounded by residential buildings, parks and schools, and is around 200 m to the west of Huju road, a heavily traveled surface street (average traffic count, ~5500 vehicles per hour with an estimated truck percentage of 3.63%). Most of the petrochemical industries and coal-fired power plants are located more than 30 km to the north of NEPB. As such, besides the regional $PM_{2.5}$ sources characterized by long-term influences and long-range transport, the NEPB site is impacted by traffic substantially.

2.2. Data collection

A Xact 625 ambient metals monitor was configured to quantify 23 elements (K, Fe, Zn, Ca, Si, Mn, Pb, Cu, Ti, As, V, Ba, Cr, Se, Ag, Cd, Ni, Au, Co, Sn, Sb, Tl, Hg, plus Pd for quality assurance). Details of the instrumentation were introduced in Chang et al. (2018) and Furger et al. (2017). Briefly, the Xact 625 ambient metals monitor is an X-ray fluorescence spectrometer designed for continuous sampling and analyzing elements in aerosol. In this work, ambient air was sampled by the Xact 625 through a $PM_{2.5}$ cyclone inlet (Model VSCC-A, BGI Inc., MA, USA) at a flow rate of 16.7 L min^{-1}. The $PM_{2.5}$ was deposited onto a Teflon filter tape. After each sampling interval, the filter tape loaded with $PM_{2.5}$ was moved and analyzed with an X-ray fluorescence spectrometer automatically, and the next sampling was initiated on a clean spot of the filter tape. This sampling and analyzing cycle was configured to be 1 h in this work, and the filter tape reel was replaced every 25 days. In the current work, the concentrations of elements measured for 0:00–1:00 a.m. at midnight were not included for analysis, as the automated internal quality control checks were programmed to take place during that period on each day (30 min).

To ensure data quality, the working conditions (e.g., flow rate) of the Xact 625 were monitored through remote login in the morning and afternoon of each day. The instrument maintenance was performed at least once a week, and the sampling flow rate and X-ray fluorescence response were calibrated periodically. Moreover, the elemental mass concentrations obtained by Xact 625 were validated by comparing to 23-h filter measurements with inductively coupled plasma-mass spectrometer (ICP-MS, Agilent, CA, USA). Details of the comparison between online Xact 625 and offline 23-h filter measurements were provided in supplementary information and Table S1.

In the current work, the hourly elements concentrations were recorded from 12/12/2016, 12:00 at noon (local time, GMT+8 h) until 12/31/2017, 23:00. The detection limits for 1-h sampling of the 23 target elements ranged from 0.2 (As) to 17.8 ng m^{-3} (Si). During the measurement campaign, several interruptions occurred due to instrument maintenance and/or power failure. The multi-element data set consists of 7025 valid 1-h samples out of 8844 theoretical samples (79.4% coverage). Missed measurements of Au, Sn, Sb, Tl, and Co accounted for more than 50% (range 63.1–100%) of the 7025 valid 1-h samples, and the concentrations of these five elements were not reported or discussed in this work. At the same sampling site, concentrations of $PM_{2.5}$ mass and gaseous pollutants (SO_2, NO_2 and CO) were also monitored at 1-h intervals during the same periods. The $PM_{2.5}$ was measured using a BAM1020 Continuous Particulate Monitor (MetOne, OR, USA). SO_2, NO_X, and CO concentrations were determined using EC9850B, EC9841B, and EC9830B, respectively. All the gaseous pollutants monitors are from Ecotech (Vic, Australia). Meteorological data, including ambient temperature (Temp), relative humidity (RH), and wind speed (WS) and direction (WD) were recorded and synchronized with elements measurements at the NEPB site. The time series for hourly concentrations of eighteen elements, $PM_{2.5}$ and gaseous pollutants, as well as the hourly values of Temp and RH are shown in Fig. S2. The

23-h, weekly and monthly patterns of elements, $PM_{2.5}$ mass, gaseous pollutants, Temp and RH are presented using boxplots in Fig. S3 – S7, from which K and Si are selected as illustrative examples and shown in Fig. 1. The WS and WD information are summarized using a wind rose plot in Fig. S8.

2.3. Preliminary source identification

The enrichment factor (EF) was calculated to assess whether a certain element had anthropogenic sources other than the natural source using Si as the reference. EFs compare elemental concentrations in ambient particles with corresponding elemental concentrations in the crust (Zoller et al., 1974; Cheung et al., 2011; Clements et al., 2014). Details for the EF calculation were provided in supplementary information. EF values close to unity indicate the dominance of crustal source, and EF values greater than 10 suggest influences from anthropogenic activities. Moreover, bivariate polar plot (BPP) and conditional probability function (CPF) plot were performed to gain a graphical impression of potential source influences at the monitoring site. In BPP, elements concentrations are shown to vary by WS and WD; the CPF plot presents which WDs are dominated by high concentrations with probability. Details of the plotting methods for BPP and CPF were given in several previous studies (Carslaw and Ropkins, 2012; Carslaw and Beevers, 2013; Chang et al., 2017; Chang et al., 2018). In this work, the BPP and CPF were performed on the hourly resolved data of eighteen elements, three gaseous pollutants and $PM_{2.5}$ mass in Figs. S9 and S10, respectively. The BPP and CPF results of Zn and Cr were selected as illustrative examples and plotted in Fig. 2.

2.4. Source apportionment

Positive matrix factorization (PMF), a multivariate receptor model, resolves the factor profiles and contributions by minimizing the sum of the squared, scaled residues (Q), and was commonly used to apportion $PM_{2.5}$ components to factors representing pollution sources or atmospheric processes (Jaeckels et al., 2007; Shrivastava et al., 2007; Xie et al., 2012; Wang et al., 2017; Wang et al., 2018). In this work, the U.S. Environmental Protection Agency (EPA) PMF version 5.0 was used as the primary source apportionment tool with three error estimation methods including bootstrapping (BS), displacement (DISP), and bootstrapping enhanced with DISP (BS-DISP) (Norris et al., 2014; Paatero et al., 2014; Brown et al., 2015).

Out of the 23 elements, Au, Co, Sn, Sb and Tl were not included for PMF analysis due to their high fractions of missing values. The measurements below detection limit (BDL) of Ag and Cd accounted for 59.2% and 86.8% of the 7025 valid 1-h samples, so they were also excluded during PMF analysis. The measurement campaign was impacted by firework burning during the Spring Festival (January 26–February 16, 2017) and sandstorm in late spring (May 6–11, 2017), resulting in spikes of several elements concentrations. As such, the PMF input data did not contain the hourly elements concentrations collected during those two events periods. The final input hourly data for PMF analysis had 6456 measurements of 16 elements (K, Fe, Zn, Ca, Si, Mn, Pb, Cu, Ti, As, V, Ba, Cr, Se, Ni and Hg), and were termed "1-h data set". The generation of uncertainty data set and treatment of missing and BDL values for PMF analysis were provided in supplementary information.

In this work, the 23-h averages of hourly elements

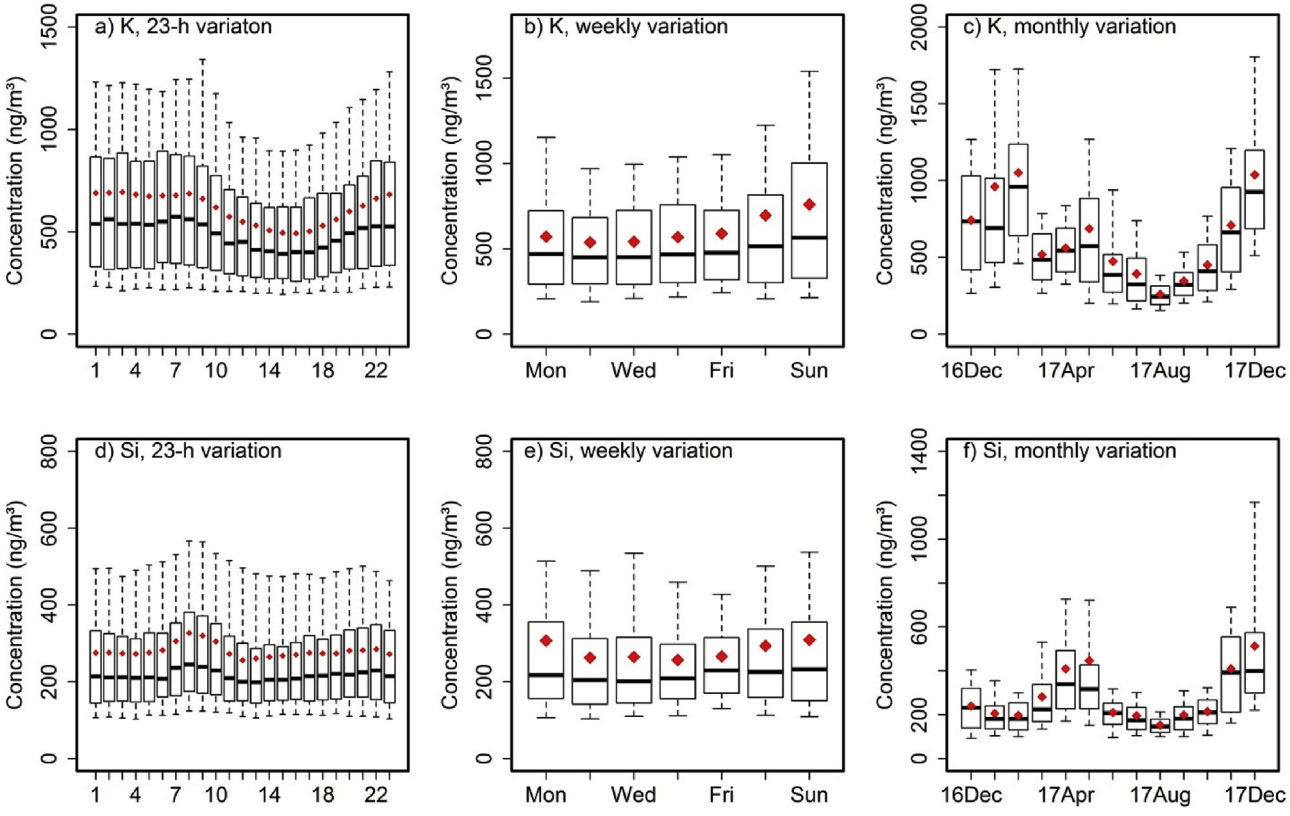

Fig. 1. Diurnal, weekly and monthly variations of K (a–c) and Si (d–f) based on hourly measurements for the whole sampling period. The boxes depict the median (dark line), inner quartile range (box), 10th and 90th percentiles (whiskers) and the mean (red diamond). (For interpretation of the references to colour in this figure legend, the reader is referred to the Web version of this article.)

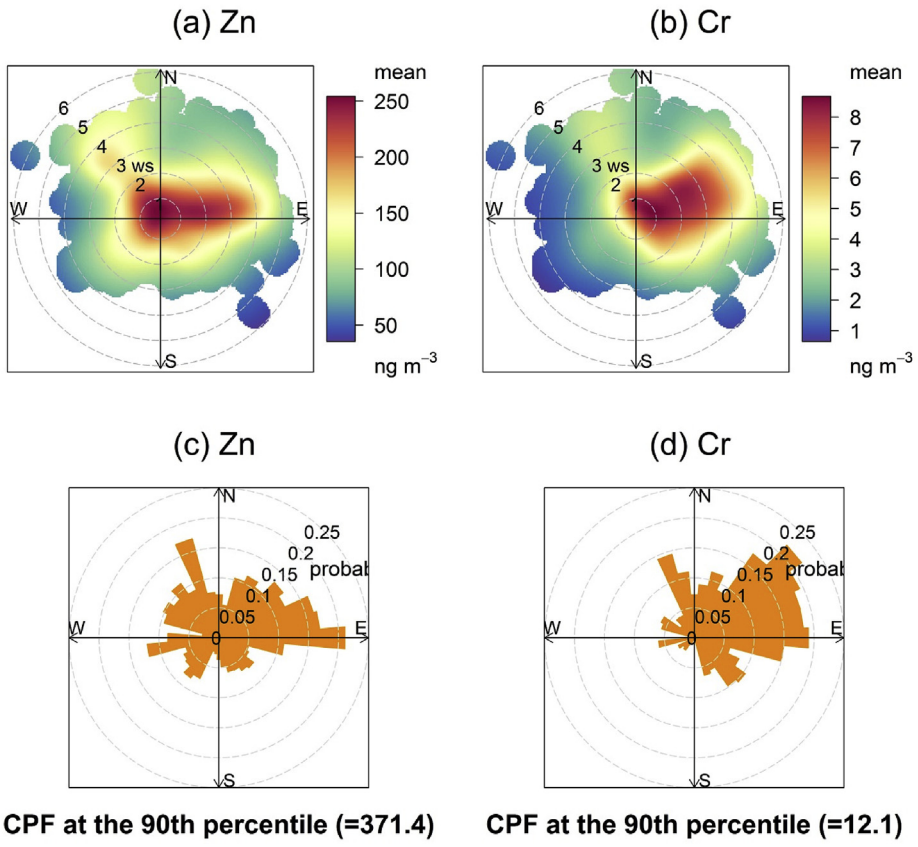

Fig. 2. Bivariate polar plots and conditional probability function plots of Zn (a, c) and Cr (b, d) concentrations for the whole sampling period.

concentrations were calculated to simulate daily filter sampling data, and were also used as inputs for PMF source apportionment. The elements data selection, uncertainty estimation, and treatments of missing and BDL values were conducted in a same manner as the 1-h data set. The final input 23-h data contained 297 daily averages of 16 elements. The PMF solutions derived from 1-h and 23-h data sets were compared to illustrate the advantage of using high time-resolved data set in source apportionment. In this work, PMF solutions using 3–9 factors were considered for both the 1-h and 23-h data sets, with the final factor number chosen primarily based on interpretability as well as the error estimation results. Details of the error estimation using BS, DISP, and BS-DISP methods were provided in supplementary information.

3. Results and discussion

3.1. Overview of Xact 625 measurements

The statistics of $PM_{2.5}$ elements concentrations detected by Xact 625, as well as the EFs are summarized in Table 1. Among the 18 elements, K, Fe, Ca, and Si were the most abundant species (average 280 ± 254–610 ± 513 ng m^{-3}), totally accounting for $80.9\% \pm 6.17\%$ of all elements concentrations during the whole period. Elements As, V, Ba, Cr, Se, Ag, Cd, Ni, and Hg had low hourly mass concentrations, with averages and medians close to or lower than 10 ng m^{-3}. The hourly concentrations of total elements accounted for $10.1 \pm 10.4\%$ of $PM_{2.5}$ mass (37.7 ± 33.8 μg m^{-3}) on average. Compared to other high time-resolved elements measurements, the average concentrations observed in this study were in similar magnitude as other mega cities in East Asia (Park et al., 2014; Chang et al., 2018; Wang et al., 2018), but were up to150 times higher than those measured in Europe and North America (Dall'Osto et al., 2013; Sofowote et al., 2015; Visser et al., 2015a; Visser et al., 2015b; Phillips-Smith et al., 2017).

In Table 1, the average EFs of K, Fe, Ca, Ti, and Ba are in the range of 9.69 ± 6.31 to 30.5 ± 71.3, suggesting that anthropogenic activities have some contributions to these elements, although they are typical crustal elements (Wu et al., 2007; Dall'Osto et al., 2013; Clements et al., 2014; Phillips-Smith et al., 2017). The other elements (e.g., Zn, As) have large EF values close to or higher than 100, indicating the dominant influences from anthropogenic activities. Fig. S9 shows the BPP results of hourly elements concentrations at the NEPB site. Nearly all elements have higher concentrations at low WS, which is reasonable at urban sites where higher pollutants concentrations are more likely associated with stable atmospheric conditions (Elminir, 2005). A number of elements also have elevated concentrations when the wind was from specific directions (Fig. S9). For example, higher concentrations of Zn, Cr, V, and Ni are more likely from east or northeast (0–45°) emissions (Figs. 2a, b and S9k, q), which might be ascribed to the heavy traffic in the east/northeast of the sampling site. The CPF was calculated to show the wind directions that dominated specified high concentrations of elements with probability. As shown in Fig. S10, the 90th percentile of elements concentrations is set as the threshold criterion. The source directions reflected by CPF were generally consistent as those inferred from BPP. For example, Zn, Cr, V, and Ni also had high CPF values with wind direction from east or northeast (Figs. 2c, d and S10k, q).

3.2. Temporal variations

The high time-resolved data obtained from Xact 625 enabled

Table 1
Statistics of hourly measurements ($N = 7025$) of ambient elements (ng m^{-3}) and their enrichment factors (EFs), $PM_{2.5}$ mass (μg m^{-3}) and gaseous pollutants (mg m^{-3}).

	Mean ± stdev[a]	median	min	max	missing%[b]	BDL%[c]	EFs[d]
K	610 ± 513	478	39.6	10055	0	0	27.7 ± 20.0
Fe	577 ± 419	470	17.7	4822	0	0	19.8 ± 9.47
Zn	199 ± 188	145	1.38	3276	0	0	3514 ± 2904
Ca	316 ± 334	236	4.43	4398	0.04	0	11.1 ± 4.30
Si	280 ± 254	216	33.6	6275	0	0	/
Mn	48.9 ± 38.3	38.8	0.30	427	0	0.014	101 ± 63.4
Pb	50.8 ± 47.6	37.5	0.81	861	0	0	3260 ± 2829
Cu	27.2 ± 38.4	18.5	2.40	1034	0	0	1375 ± 1770
Ti	25.9 ± 24.2	20.1	1.07	442	0.67	0	9.69 ± 6.31
As	11.9 ± 11.0	9.05	0.030	182	1.64	0.26	9493 ± 7714
V	6.05 ± 5.90	4.08	0.064	65.9	12.0	1.85	144 ± 146
Ba	13.8 ± 39.2	7.21	0.0030	1055	2.38	6.14	30.5 ± 71.3
Cr	6.00 ± 6.82	3.96	0.0040	94.6	0.40	3.36	219 ± 259
Se	5.15 ± 3.82	4.23	0.0020	33.7	0.19	0.53	127 ± 77.5
Ag	7.54 ± 2.45	7.18	1.33	20.2	0.00	59.2	239296 ± 167784
Cd	6.99 ± 2.88	6.71	0.30	33.1	0.01	86.8	112 ± 87.8
Ni	3.62 ± 3.49	2.63	0.0010	45.9	0.10	2.18	253 ± 253
Hg	2.04 ± 1.22	1.90	0.0010	10.2	0.73	4.58	NA[e]
$PM_{2.5}$	37.7 ± 33.8	29.0	3.00	341	0.45	0	
SO_2	0.019 ± 0.014	0.016	0.0010	0.61	0.47	0.028	
NO_2	0.045 ± 0.024	0.040	0.0010	0.16	0.87	0.014	
CO	0.96 ± 0.49	0.91	0.038	9.28	0.23	0.13	
RH (%)	60.3 ± 17.8	61.0	16.0	94.0	1.04		
Temp. (°C)	17.6 ± 9.35	17.4	−1.40	40.3	1.15		

[a] Standard deviation.
[b] Missing% = No. of missed observations/7025, the missed observations were not included for data analysis.
[c] BDL% = No. of measurements below detection limit/7025, the BDL measurements were included for data analysis.
[d] Average ± standard deviation, where Si is used as the reference element; [e] the average mass content of Hg in upper continental crust (UCC) is not available.

the visualization of elements diurnal variation. In Figs. S3–S6, the 23-h variations of elements are exhibited using boxplots. Except Cd and Ag, all the elements had elevated hourly median concentrations in the morning (6:00–10:00) and evening (18:00–21:00), and decreased concentrations in the afternoon (13:00–16:00). However, due to the difference in emission sources, the diurnal patterns of elements concentrations are not exactly the same. The peak concentrations of Fe, Ca, and Si in the morning (Figs. S3d, j and 1d) reflected the influence of traffic during rush-hour times. Elements Zn, Pb, and As showed a sinusoidal pattern (Figs. S3g, S4g, and S5a), which is likely shaped by constant industrial emissions and the changes in planetary boundary layer height (PBLH). In this work, nearly all elements had lowest concentrations at around 13:00–16:00, when the ambient temperature (Fig. S7m) and PBLH (Zhang and Cao, 2015) are both the highest during the day.

In Figs. S3–S6, the weekly variations are calculated based on hourly elements concentrations and no weekend decrease has been observed for any element. One possible explanation is that the NEPB site is located in the downtown area where the traffic and industrial influences have little weekday-weekend variation, as supported by the weekly patterns of SO_2, NO_2, and CO (Figs. S7b, e, h). Figs. S3–S6 also provide the monthly variations of elements concentrations, mostly exhibiting summertime decreases and wintertime elevations, which is partly associated with the lower PBLH in winter than in summer (Venzac et al., 2009; Seidel et al., 2012). No seasonal trend was observed for Ag and Cd (Figs. S6c and f), and this might be due to their high fractions of BDL measurements. The elevated concentrations of many elements, especially for crustal species (e.g., Fe, Ca, Si, Ti) in spring (March–May) can be attributed to the drier conditions (Fig. S7l) favoring the re-suspension of mineral dust and the influences of sandstorm (Zhao et al., 2008; Zhang et al., 2018). Firework combustion can emit particles enriched with Ba and K (Moreno et al., 2010; Kong et al., 2015; Furger et al., 2017). The monthly average concentrations of Ba and K in January and February (Figs. S5i and 1c) were dominated by the firework events between the 2017 Chinese Spring Festival (SF) and Lantern Festival (LF) (Figs. S2a and l).

3.3. Influences from firework and sandstorm events

As mentioned above, predominant firework emissions were identified with the hourly measurements of Ba and K. In this work, the firework period was postulated to be continuous from the first increase in Ba (>20 ng m^{-3}) on January 26, 2017 to February 16, 2017. The peak hourly concentrations of Ba (0.49–1.06 μg m^{-3}) and K (5.21–10.1 μg m^{-3}) were observed between January 27, 21:00 LT and January 28, 2017 3:00 LT, during the Chinese New Year's Eve, when the most intensive firework event occurred across the nation. However, burning firework was prohibited in the urban area of Nanjing city since January 1st, 2015, so the firework emissions observed at the sampling site in this work should come from the surrounding suburban and rural areas. The 23-h patterns of Ba and K during the firework and non-firework periods were compared in Fig. S11, suggesting increased firework events at midnight during the SF period. The ratios of hourly average concentrations of elements and EFs during the firework periods to the rest of the measurements ("non-firework periods") are presented in Fig. 3. The hourly average concentrations of Ba (78.7 ± 139.5 ng m^{-3}) and K (1382 ± 1226 ng m^{-3}) during the firework periods are 8.26 and 2.46 times higher than non-firework periods (Fig. 3a). While the hourly average $PM_{2.5}$ concentration only increased by 43%, supporting that firework emissions were enriched with Ba and K (Fig. 3b). Significant elevations ($p < 0.01$) in hourly average concentrations were also observed for Pb and Hg (19–28%) during the firework periods, which is likely related to the enhancement in $PM_{2.5}$ concentrations. Due to the holiday effect, the hourly average concentrations of elements related to crustal dust (Fe, Ca, Si, and Ti) and industrial or traffic activities (Zn, Mn, V, Cr, and Ni) were depleted by 30–50%.

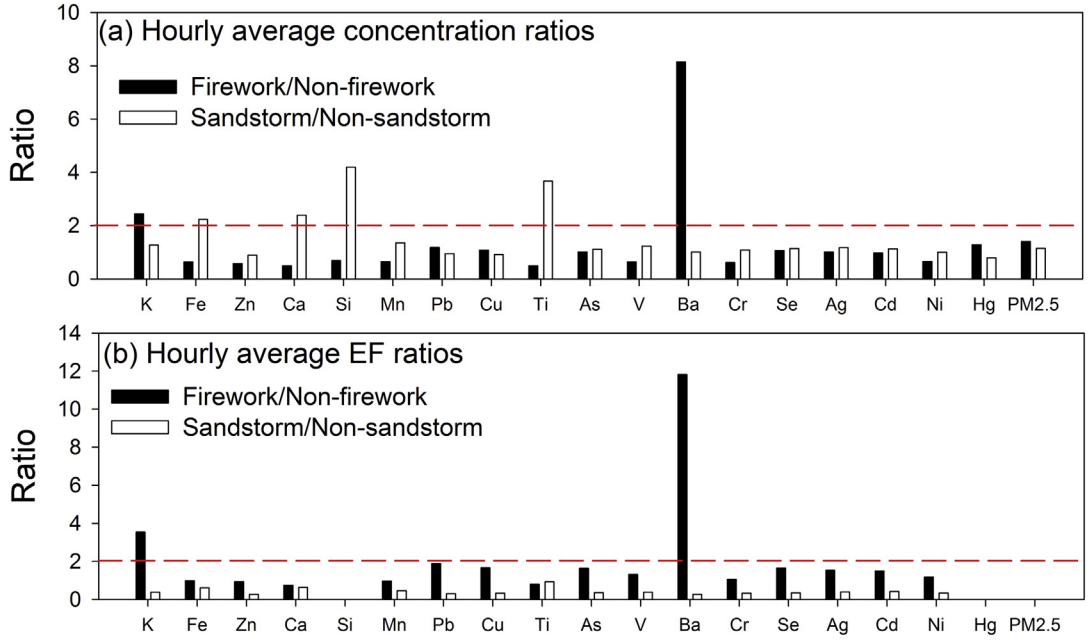

Fig. 3. Hourly average elements (a) concentrations and (b) EFs ratios for firework/non-firework and sandstorm/non-sandstorm periods.

Zhang et al. (2018) reported a severe sandstorm event originating from Gobi Desert in Central and East Asia during May 2–7, 2017, and analyzed the transport and influences of dust using simulation techniques. The hourly measurements of elements in this work also captured the influences from the sandstorm event, which was supposed to start from May 6, 2017, with substantial increases of Fe, Ca, Si, and Ti concentrations, to May 11, 2017. The peak concentrations of Fe (4.82 $\mu g\,m^{-3}$), Ca (4.40 $\mu g\,m^{-3}$), Si (6.28 $\mu g\,m^{-3}$), and Ti (442 $ng\,m^{-3}$) were observed on May 6, 2017, when the PM_{10} concentrations in Shanghai and Nanjing tripled as compared with preceding days (Zhang et al., 2018). However, the hourly average concentration of $PM_{2.5}$ during the sandstorm periods was only 15% ($p < 0.01$) higher than non-sandstorm periods, suggesting the dominance of coarse particles ($PM_{2.5\text{-}10}$) during sandstorm periods. In this work, elements concentrations were only measured in $PM_{2.5}$, and the sandstorm event would be better visible if PM_{10} mass and associated elements concentrations were obtained. The hourly average concentrations of Fe, Ca, Si, and Ti during the sandstorm periods were 2.23 (Fe) – 4.14 (Si) times higher than non-sandstorm periods (Fig. 3a). Other elements with more contributions from anthropogenic emissions (e.g., Zn, Pb) had comparable concentrations between sandstorm and non-sandstorm periods (Fig. 3a). Since Si had the highest elevation from non-sandstorm to sandstorm periods and was used as the reference for EF calculation, all elements showed lower EFs during the sandstorm periods than non-sandstorm periods with EFs ratios ranging from 0.27 (Zn) to 0.93 (Ti) (Fig. 3b). During the sandstorm periods, Ca had the lowest hourly average EF (7.22), followed by Ba (8.63), Ti (9.01), K (10.6) and Fe (12.2). The high EFs for crustal elements (~10) in this work might be explained by the fact that only $PM_{2.5}$ elements were measured, which is more influenced by anthropogenic activities than elements in coarse particles (Upadhyay et al., 2011; Clements et al., 2014).

3.4. Overview of PMF results

The 4- to 6-factor solutions were chosen for the PMF analysis with the 1-h data set ($PMF_{1\text{-}h}$ solution) as they had interpretable resulting factors and acceptable error estimation diagnostics. For each of the three $PMF_{1\text{-}h}$ solutions, all factors were mapped in >90% of BS runs ($N = 100$), and nearly no factor swapping was found for DISP and BS-DISP analysis (Tables S2–S4). The 7-factor solution contained a factor that did not have distinctive groupings of compounds (Fig. S12g). Other details on error estimation and factor number determination were provided in supplementary information. Fig. 4 compares the normalized factor profiles of the 4- to 6-factor solutions, and the factor profiles have been normalized by:

$$F^{*}_{kj} = \frac{F_{kj}}{\sum_{k=1}^{p} F_{kj}} \quad (1)$$

where F is relative weighting of species j in factor k to all other factors. The hourly resolved factor contributions of the three PMF solutions are presented in Figs. S13–S15. Figs. S16–S18 show the 23-h variations of individual factor contributions of the 4- to 6-factor solutions, and the corresponding monthly variations are summarized in Figs. S19–S21. The overall factor contributions agreed with the sum of input elements concentrations (PMF simulation/input = 0.90 ± 0.10–0.93 ± 0.09, $r > 0.95$, $p < 0.01$). The four factors linked with coal burning, crustal dust, heavy oil combustion and motor vehicle emission were resolved in all the three $PMF_{1\text{-}h}$ solutions (Fig. 4). The 5-factor solution contained a factor related to mechanical abrasion, and an Hg emission factor was identified from the 6-factor solution. The crustal dust had the highest average contribution (37.5 ± 17.3–42.7 ± 19.0%) to total elements mass, followed by the coal burning (17.6 ± 12.1–27.2 ± 15.8%) and motor vehicle emission (13.4 ± 9.76–17.2 ± 10.5%) factors.

To compare with the $PMF_{1\text{-}h}$ solutions, four to six factors were also selected for PMF solutions determined with the 23-h data set ($PMF_{23\text{-}h}$ solution). Except the motor vehicle emission factor in the 4-factor solution, all factors across the three $PMF_{23\text{-}h}$ solutions were mapped in >90% of BS runs ($N = 100$), and no factor swapping was observed for DISP analysis (Tables S5–S7). However, the 6-factor $PMF_{23\text{-}h}$ solution had a number of swaps for BS-DISP analysis with only 58% of the BS-DISP runs accepted (Table S7). The

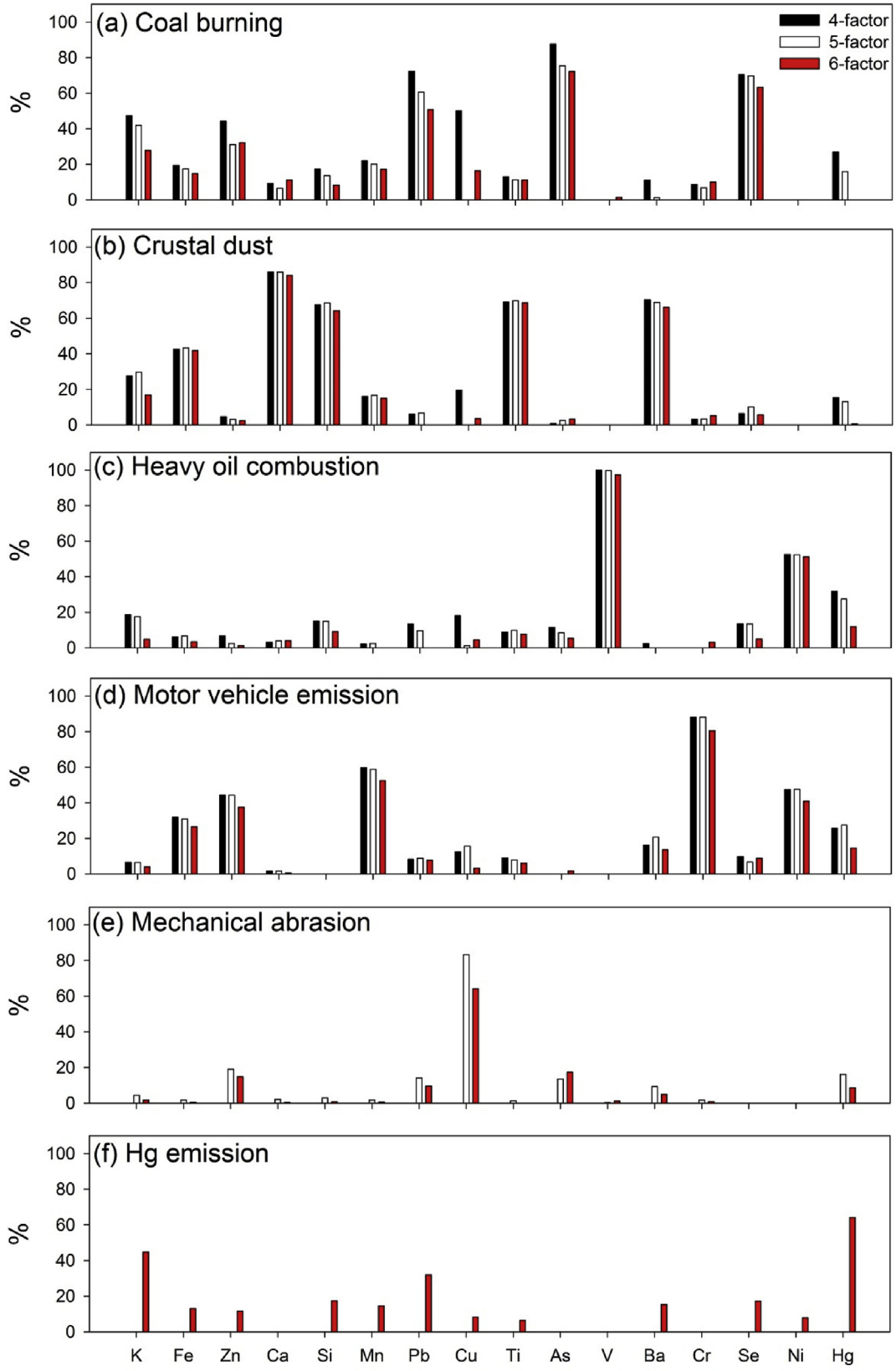

Fig. 4. Normalized factor profiles of the 4- to 6-factor $PMF_{1\text{-}h}$ solutions.

normalized factor profiles of the 4- to 6-factor $PMF_{23\text{-}h}$ solutions are provided in Fig. S22, and the overall factor contributions also reproduced the total mass of input elements (PMF simulation/input = 0.94 ± 0.069–0.95 ± 0.067, $r > 0.95$, $p < 0.01$). The time series and monthly variations of individual factor contributions of the 4- to 6-factor solutions are visualized in Figs. S23–S25 and S26–S28, respectively. The input data for PMF analysis did not include those impacted by firework emissions (January 26–February 16, 2017), and the hourly measurements were missed for more than 50% during each day from February 17 to 27, 2017. So the 23-h average concentrations of elements are only available for February 28, 2017 and the factor contributions during February 2017 are not shown in any plots of Figs. S26–S28.

3.5. Interpretation of $PMF_{1\text{-}h}$ solutions

In the 4-factor solution, the coal burning factor was characterized by the highest loadings of As, Se, and Pb (Fig. 4a), and exhibited higher contributions in cold than in warm seasons (Figs. S13a and S19a). This factor also had the strongest correlation with SO_2 ($r = 0.52$, $p < 0.01$) among the 4 factors, supporting the association of this factor with coal burning. The 23-h pattern of the factor contributions had a unimodal distribution with a broad peak in the morning (Fig. S16), which might be ascribed to the accumulation of elements from coal burning in the boundary layer during night time and atmospheric dilution after sunrise with increased boundary layer height. Besides As, Se, and Pb, typical trace elements from coal burning (Tian et al., 2011; Tian et al., 2012; Tian et al., 2014; Cao et al., 2014), the coal burning factor also had substantial contributions to K and Zn in this work. K in $PM_{2.5}$ was commonly related to biomass burning or fugitive dust (Dall'Osto et al., 2013; Clements et al., 2014; Phillips-Smith et al., 2017). However, K can also exist as K_2O (0.30–046 wt%) in coal fly ash (Koukouzas et al., 2006; Dai et al., 2010), which might be one explanation for the high loadings of K in the coal burning factor. The crustal dust factor consisted mainly of Fe, Ca, Si, and Ti (Fig. 4b), and had elevated factor contributions in both spring and winter (Figs. S13b and S19b). As mentioned before, the elevated contributions of crustal elements in spring and winter might be attributed to dry atmospheric conditions and low PBLH, respectively. Unlike other three factors, the 23-h pattern of the crustal dust factor exhibited a drop from midnight (23:00) to early morning (5:00) (Fig. S16b), which is possibly due to the decrease in traffic or construction activities during the second half of the night. The heavy oil combustion factor was distinguished by the highest percentages of V ad Ni (Fig. 4c), two tracers for the combustion process of heavy oil (Jang et al., 2007; Becagli et al., 2012). Similar as the coal burning factor, the 23-h variations of the heavy oil combustion factor also had a sinusoidal pattern (Fig. S16c). The motor vehicle emission factor was dominated by Cr and Mn, and contained substantial percentages of Fe, Zn, Ni, and Hg (Fig. 4d). The factor contributions correlated significantly with NO_2 ($r = 0.46$, $p < 0.01$) and CO ($r = 0.41$, $p < 0.01$) with similar 23-h pattern (Figs. S7d,g and S16d), reflecting the influences from traffic during rush-hour times in the morning and evening.

Besides the four factors mentioned above, an additional factor was identified with the highest fractions of Cu when the factor number increased to 5 (Fig. 4), and was linked with mechanical abrasion. Because the 23-h variations of its median factor contributions were similar as the motor vehicle emission factor

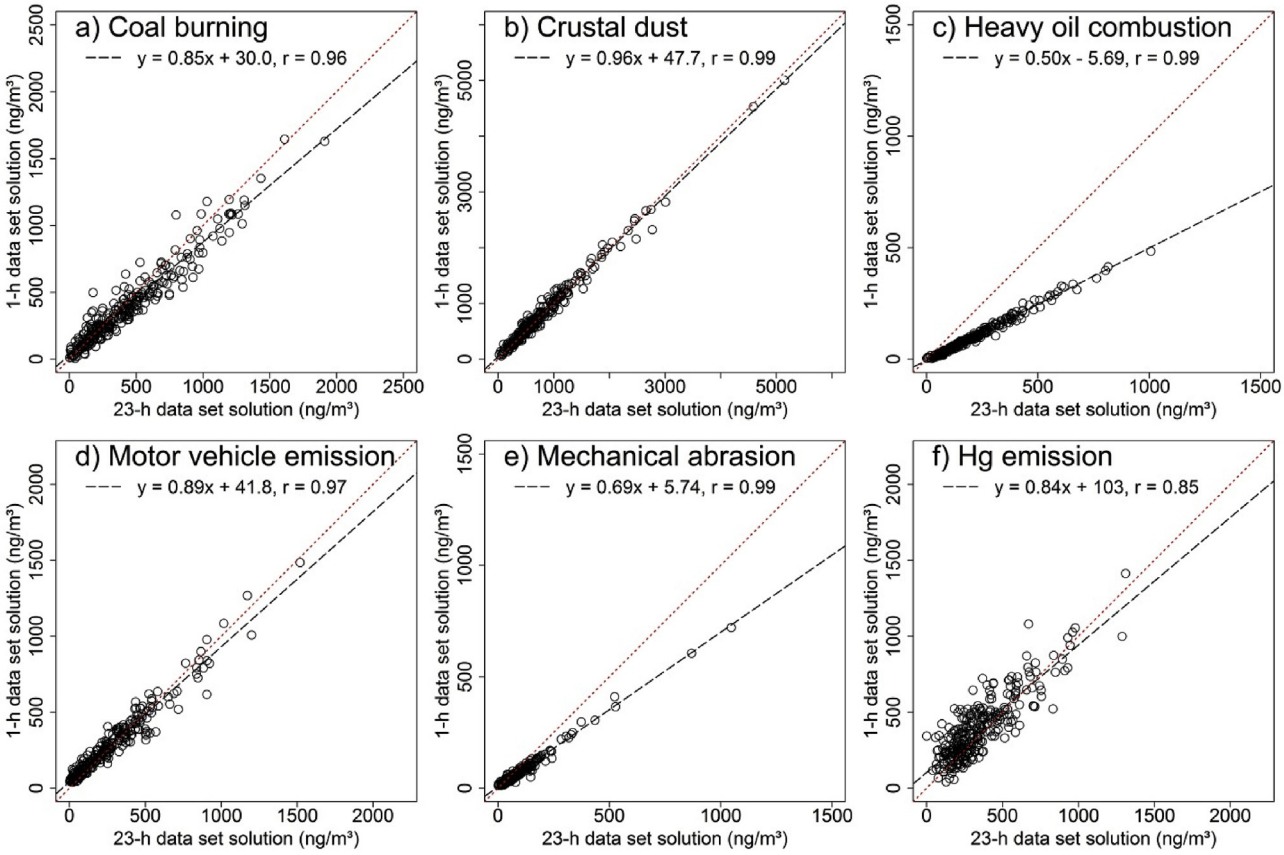

Fig. 5. Linear regressions of factor contributions for pairs of matched factors between 6-factor $PMF_{1\text{-}h}$ and 6-factor $PMF_{23\text{-}h}$ solutions.

(Figs. S17d and e), and Cu in $PM_{2.5}$ can be linked with the mechanical abrasion of brake and tire wear (McKenzie et al., 2009). In the 6-factor $PMF_{1\text{-}h}$ solution, an Hg emission factor was identified consisting mainly of Hg, K, and Pb (Fig. 4). This factor was likely related to coal combustion and non-ferrous metals smelting, which are the two major Hg emission categories in China (Streets et al., 2005; Zhang et al., 2015).

3.6. $PMF_{1\text{-}h}$ vs. $PMF_{23\text{-}h}$ solutions

The factors identified in $PMF_{23\text{-}h}$ solutions were matched to those from $PMF_{1\text{-}h}$ solutions based on factor profiles and temporal patterns of factor contributions. The 23-h average factor contributions of the $PMF_{1\text{-}h}$ solutions were calculated and regressed with the factor contributions of the $PMF_{23\text{-}h}$ solutions with 4–6 factors (Figs. S29, S30 and 5). The 4-factor $PMF_{23\text{-}h}$ and $PMF_{1\text{-}h}$ solutions had consistent factor profiles (Figs. 4 and S22) and monthly variations in factor contributions (Figs. S19 and S26). In Fig. S29, the factor contributions of all four factors were strongly correlated ($r = 0.93–0.99$, $p < 0.01$) between the $PMF_{1\text{-}h}$ vs. $PMF_{23\text{-}h}$ solutions. The contributions of the heavy oil combustion factor in the $PMF_{1\text{-}h}$ solution were around half of those derived from the $PMF_{23\text{-}h}$ solution (Fig. S29c). This is because the heavy oil combustion factor of the $PMF_{23\text{-}h}$ solution contains higher fractions of major $PM_{2.5}$ elements (e.g., K, Fe, Zn, Ca, and Si) in this work (Figs. S22c and 4c). Unlike the 5-factor $PMF_{1\text{-}h}$ solution, an Hg emission factor, but not the mechanical abrasion factor, was identified in the 5-factor $PMF_{23\text{-}h}$ solution (Fig. S22f). So only four out of the five factors were matched and correlated ($r = 0.93–0.99$, $p < 0.01$) between the 5-factor $PMF_{1\text{-}h}$ and 5-factor $PMF_{23\text{-}h}$ solutions (Fig. S30). The Hg emission factor in the $PMF_{23\text{-}h}$ solution contributed an average of $25.7 \pm 13.4\%$ to the total elements mass, much higher than mechanical abrasion factor ($5.85 \pm 6.09\%$) in the $PMF_{1\text{-}h}$ solution, which might be one reason for the difference in coal burning factor contributions between the two PMF solutions (Fig. S30a). When the factor number increased to 6, all factors determined with the 23-h data set could be matched and correlated ($r = 0.85–0.99$, $p < 0.01$) with those from the $PMF_{1\text{-}h}$ solution (Fig. 5). However, the Hg emission factor of the $PMF_{1\text{-}h}$ and $PMF_{23\text{-}h}$ solutions have distinct loadings of Pb (Figs. 4f and S22f), and the regression plot of the Hg emission factor (Fig. 5f) is more scattered that other factors with the lowest correlation coefficient ($r = 0.85$), suggesting that the contributions of coal burning factor are partially misclassified as Hg emission factor during the PMF analysis with 23-h data set.

4. Conclusions

In this work, the hourly measurements of $PM_{2.5}$ elements concentrations enabled the identification of the influences from local aerosol sources (e.g., traffic related) at specific time during the day. For example, the increase of crustal elements (e.g., Fe, Ca, and Si) concentrations in the morning suggested an influence from road dust resuspension due to traffic activities. The diurnal and monthly variations of elements concentrations reflected a mixture of influences from different emission sources and the changes in meteorological conditions (e.g., PBLH). As such, high time-resolved measurements data (e.g., 1-h) with greater inter-sample variability should be more capable in extracting the impacts of specific emission sources than long-time integrated sampling (e.g., daily), and two data sets of elements concentrations with different time resolution (1-h and 23-h) were applied for source apportionment by using PMF model. The 4- and 6-factor $PMF_{23\text{-}h}$ solutions had similar factor profiles and consistent factor contributions as the corresponding $PMF_{1\text{-}h}$ solutions. These similarities provided reassurance on the identity of the sources. Although the PMF analysis with 23-h data set can also identify local as well as regional sources, it misclassified some elements to certain factors, leading to substantial difference in absolute factor contributions between $PMF_{23\text{-}h}$ and $PMF_{1\text{-}h}$ solutions. For example, the 4-factor $PMF_{23\text{-}h}$ solution over-attributed a number of major elements (e.g., K, Fe, Zn, Ca, and Si) to the heavy oil combustion factor, and the 6-factor $PMF_{23\text{-}h}$ solution misclassified Pb to the Hg emission factor, which might be ascribed to the reduced inter-sample variability in the 23-h averaged data set. These results support the use of high time-resolved measurements data for PMF analysis to obtain valid and robust source apportionment results.

Declaration of interests

The authors declare that they have no known competing financial interests or personal relationships that could have appeared to influence the work reported in this paper.

Conflicts of interest

The authors declare that they have no conflict of interest.

Acknowledgements

This work was supported by the National Key Research and Development Program of China (2016YFC0208504); National Natural Science Foundation of China (NSFC, 41701551); the State Key Laboratory of Pollution Control and Resource Reuse Foundation (No. PCRRF17040), China; the Startup Foundation for Introducing Talent of NUIST (No. 2243141801001), China.

Appendix A. Supplementary data

Supplementary data to this article can be found online at https://doi.org/10.1016/j.envpol.2019.07.096.

References

Becagli, S., Sferlazzo, D.M., Pace, G., di Sarra, A., Bommarito, C., Calzolai, G., Ghedini, C., Lucarelli, F., Meloni, D., Monteleone, F., Severi, M., Traversi, R., Udisti, R., 2012. Evidence for heavy fuel oil combustion aerosols from chemical analyses at the island of Lampedusa: a possible large role of ships emissions in the Mediterranean. Atmos. Chem. Phys. 12, 3479–3492. https://doi.org/10.5194/acp-12-3479-2012.

Bell, M.L., Ebisu, K., Leaderer, B.P., Gent, J.F., Lee, H.J., Koutrakis, P., Wang, Y., Dominici, F., Peng, R.D., 2014. Associations of PM(2.5) constituents and sources with hospital admissions: analysis of four counties in Connecticut and Massachusetts (USA) for persons ≥ 65 years of age. Environ. Health Perspect. 122, 138–144. https://doi.org/10.1289/ehp.1306656.

Brown, S.G., Eberly, S., Paatero, P., Norris, G.A., 2015. Methods for estimating uncertainty in PMF solutions: examples with ambient air and water quality data and guidance on reporting PMF results. Sci. Total Environ. 518–519, 626–635. https://doi.org/10.1016/j.scitotenv.2015.01.022.

Cao, S., Duan, X., Zhao, X., Ma, J., Dong, T., Huang, N., Sun, C., He, B., Wei, F., 2014. Health risks from the exposure of children to As, Se, Pb and other heavy metals near the largest coking plant in China. Sci. Total Environ. 472, 1001–1009. https://doi.org/10.1016/j.scitotenv.2013.11.124.

Carslaw, D.C., Ropkins, K., 2012. Openair—an R package for air quality data analysis. Environ. Model. Softw. 27, 52–61.

Carslaw, D.C., Beevers, S.D., 2013. Characterising and understanding emission sources using bivariate polar plots and k-means clustering. Environ. Model. Softw. 40, 325–329.

Chang, Y., Deng, C., Cao, F., Cao, C., Zou, Z., Liu, S., Lee, X., Li, J., Zhang, G., Zhang, Y., 2017. Assessment of carbonaceous aerosols in Shanghai, China – Part 1: long-term evolution, seasonal variations, and meteorological effects. Atmos. Chem. Phys. 17, 9945–9964. https://doi.org/10.5194/acp-17-9945-2017.

Chang, Y., Huang, K., Xie, M., Deng, C., Zou, Z., Liu, S., Zhang, Y., 2018. First long-term and near real-time measurement of trace elements in China's urban atmosphere: temporal variability, source apportionment and precipitation effect. Atmos. Chem. Phys. 18, 11793–11812. https://doi.org/10.5194/acp-18-11793-2018.

Cheung, K., Daher, N., Kam, W., Shafer, M.M., Ning, Z., Schauer, J.J., Sioutas, C., 2011. Spatial and temporal variation of chemical composition and mass closure of

ambient coarse particulate matter (PM10–2.5) in the Los Angeles area. Atmos. Environ. 45, 2651–2662.
Cho, W.-S., Duffin, R., Poland, C.A., Duschl, A., Oostingh, G.J., MacNee, W., Bradley, M., Megson, I.L., Donaldson, K., 2012. Differential pro-inflammatory effects of metal oxide nanoparticles and their soluble ions in vitro and in vivo; zinc and copper nanoparticles, but not their ions, recruit eosinophils to the lungs. Nanotoxicology 6, 22–35. https://doi.org/10.3109/17435390.2011.552810.
Clements, N., Eav, J., Xie, M., Hannigan, M.P., Miller, S.L., Navidi, W., Peel, J.L., Schauer, J.J., Shafer, M.M., Milford, J.B., 2014. Concentrations and source insights for trace elements in fine and coarse particulate matter. Atmos. Environ. 89, 373–381.
Dai, S., Zhao, L., Peng, S., Chou, C.-L., Wang, X., Zhang, Y., Li, D., Sun, Y., 2010. Abundances and distribution of minerals and elements in high-alumina coal fly ash from the Jungar Power Plant, Inner Mongolia, China. Int. J. Coal Geol. 81, 320–332.
Dall'Osto, M., Querol, X., Amato, F., Karanasiou, A., Lucarelli, F., Nava, S., Calzolai, G., Chiari, M., 2013. Hourly elemental concentrations in PM2.5 aerosols sampled simultaneously at urban background and road site during SAPUSS – diurnal variations and PMF receptor modelling. Atmos. Chem. Phys. 13, 4375–4392. https://doi.org/10.5194/acp-13-4375-2013.
Dockery, D.W., Pope, C.A., Xu, X., Spengler, J.D., Ware, J.H., Fay, M.E., Ferris, B.G., Speizer, F.E., 1993. An association between air pollution and mortality in six U.S. cities. N. Engl. J. Med. 329, 1753–1759. https://doi.org/10.1056/NEJM199312093292401.
Elminir, H.K., 2005. Dependence of urban air pollutants on meteorology. Sci. Total Environ. 350, 225–237. https://doi.org/10.1016/j.scitotenv.2005.01.043.
Furger, M., Minguillón, M.C., Yadav, V., Slowik, J.G., Hüglin, C., Fröhlich, R., Petterson, K., Baltensperger, U., Prévôt, A.S., 2017. Elemental composition of ambient aerosols measured with high temporal resolution using an online XRF spectrometer. Atmos. Meas. Tech. 10, 2061.
Ito, K., Christensen, W.F., Eatough, D.J., Henry, R.C., Kim, E., Laden, F., Lall, R., Larson, T.V., Neas, L., Hopke, P.K., Thurston, G.D., 2006. PM source apportionment and health effects: 2. An investigation of intermethod variability in associations between source-apportioned fine particle mass and daily mortality in Washington, DC. J. Expo. Sci. Environ. Epidemiol. 16, 300–310. https://doi.org/10.1038/sj.jea.7500464.
Jaeckels, J.M., Bae, M.S., Schauer, J.J., 2007. Positive matrix factorization (PMF) analysis of molecular marker measurements to quantify the sources of organic aerosols. Environ. Sci. Technol. 41, 5763–5769. https://doi.org/10.1021/es062536b.
Jang, H.-N., Seo, Y.-C., Lee, J.-H., Hwang, K.-W., Yoo, J.-I., Sok, C.-H., Kim, S.-H., 2007. Formation of fine particles enriched by V and Ni from heavy oil combustion: anthropogenic sources and drop-tube furnace experiments. Atmos. Environ. 41, 1053–1063. https://doi.org/10.1016/j.atmosenv.2006.09.011.
Kim, E., Hopke, P.K., Kenski, D.M., Koerber, M., 2005a. Sources of fine particles in a rural Midwestern U.S. area. Environ. Sci. Technol. 39, 4953–4960. https://doi.org/10.1021/es0490774.
Kim, E., Hopke, P.K., Pinto, J.P., Wilson, W.E., 2005b. Spatial variability of fine particle mass, components, and source contributions during the regional air pollution study in St. Louis. Environ. Sci. Technol. 39, 4172–4179. https://doi.org/10.1021/es049824x.
Kong, S.F., Li, L., Li, X.X., Yin, Y., Chen, K., Liu, D.T., Yuan, L., Zhang, Y.J., Shan, Y.P., Ji, Y.Q., 2015. The impacts of firework burning at the Chinese Spring Festival on air quality: insights of tracers, source evolution and aging processes. Atmos. Chem. Phys. 15, 2167–2184. https://doi.org/10.5194/acp-15-2167-2015.
Koukouzas, N.K., Zeng, R., Perdikatsis, V., Xu, W., Kakaras, E.K., 2006. Mineralogy and geochemistry of Greek and Chinese coal fly ash. Fuel 85, 2301–2309.
Laden, F., Neas, L.M., Dockery, D.W., Schwartz, J., 2000. Association of fine particulate matter from different sources with daily mortality in six U.S. cities. Environ. Health Perspect. 108, 941–947.
Li, R., Ning, Z., Majumdar, R., Cui, J., Takabe, W., Jen, N., Sioutas, C., Hsiai, T., 2010. Ultrafine particles from diesel vehicle emissions at different driving cycles induce differential vascular pro-inflammatory responses: implication of chemical components and NF-κB signaling, Part. Fibre Toxicol. 7 (6) https://doi.org/10.1186/1743-8977-7-6.
Marcazzan, G.M., Vaccaro, S., Valli, G., Vecchi, R., 2001. Characterisation of PM10 and PM2.5 particulate matter in the ambient air of Milan (Italy). Atmos. Environ. 35, 4639–4650. https://doi.org/10.1016/S1352-2310(01)00124-8.
McKenzie, E.R., Money, J.E., Green, P.G., Young, T.M., 2009. Metals associated with stormwater-relevant brake and tire samples. Sci. Total Environ. 407, 5855–5860. https://doi.org/10.1016/j.scitotenv.2009.07.018.
Moreno, T., Querol, X., Alastuey, A., Amato, F., Pey, J., Pandolfi, M., Kuenzli, N., Bouso, L., Rivera, M., Gibbons, W., 2010. Effect of fireworks events on urban background trace metal aerosol concentrations: is the cocktail worth the show? J. Hazard. Mater. 183, 945–949.
Norris, G., Duvall, R., Brown, S., Bai, S., 2014. EPA Positive Matrix Factorization (PMF) 5.0 Fundamentals and User Guide Prepared for the. US Environmental Protection Agency Office of Research and Development, Washington, DC.
Paatero, P., Eberly, S., Brown, S., Norris, G., 2014. Methods for estimating uncertainty in factor analytic solutions. Atmos. Meas. Tech. 7, 781.
Park, S.S., Cho, S.Y., Jo, M.R., Gong, B.J., Park, J.S., Lee, S.J., 2014. Field evaluation of a near–real time elemental monitor and identification of element sources observed at an air monitoring supersite in Korea. Atmos. Pollut. Res. 5, 119–128. https://doi.org/10.5094/APR.2014.015.
Phillips-Smith, C., Jeong, C.H., Healy, R.M., Dabek-Zlotorzynska, E., Celo, V., Brook, J.R., Evans, G., 2017. Sources of particulate matter components in the Athabasca oil sands region: investigation through a comparison of trace element measurement methodologies. Atmos. Chem. Phys. 17, 9435–9449. https://doi.org/10.5194/acp-17-9435-2017.
Pope, C.A., Burnett, R.T., Thun, M.J., Calle, E.E., Krewski, D., Ito, K., Thurston, G.D., 2002. Lung cancer, cardiopulmonary mortality, and long-term exposure to fine particulate air pollution. J. Am. Med. Assoc. 287, 1132–1141. https://doi.org/10.1001/jama.287.9.1132.
Pope, C.A., Dockery, D.W., 2006. Health effects of fine particulate air pollution: lines that connect. J. Air Waste Manag. Assoc. 56, 709–742.
Qin, Y., Kim, E., Hopke, P.K., 2006. The concentrations and sources of PM2.5 in metropolitan New York City. Atmos. Environ. 40, 312–332. https://doi.org/10.1016/j.atmosenv.2006.02.025.
Seidel, D.J., Zhang, Y., Beljaars, A., Golaz, J.C., Jacobson, A.R., Medeiros, B., 2012. Climatology of the planetary boundary layer over the continental United States and Europe. J. Geophys. Res. Atmos. 117.
Shrivastava, M.K., Subramanian, R., Rogge, W.F., Robinson, A.L., 2007. Sources of organic aerosol: positive matrix factorization of molecular marker data and comparison of results from different source apportionment models. Atmos. Environ. 41, 9353–9369. https://doi.org/10.1016/j.atmosenv.2007.09.016.
Sofowote, U.M., Su, Y., Dabek-Zlotorzynska, E., Rastogi, A.K., Brook, J., Hopke, P.K., 2015. Sources and temporal variations of constrained PMF factors obtained from multiple-year receptor modeling of ambient PM2. 5 data from five speciation sites in Ontario, Canada. Atmos. Environ. 108, 140–150.
Stanek, L.W., Sacks, J.D., Dutton, S.J., Dubois, J.-J.B., 2011. Attributing health effects to apportioned components and sources of particulate matter: an evaluation of collective results. Atmos. Environ. 45, 5655–5663. https://doi.org/10.1016/j.atmosenv.2011.07.023.
Streets, D.G., Hao, J., Wu, Y., Jiang, J., Chan, M., Tian, H., Feng, X., 2005. Anthropogenic mercury emissions in China. Atmos. Environ. 39, 7789–7806. https://doi.org/10.1016/j.atmosenv.2005.08.029.
Tian, H., Wang, Y., Xue, Z., Qu, Y., Chai, F., Hao, J., 2011. Atmospheric emissions estimation of Hg, As, and Se from coal-fired power plants in China, 2007. Sci. Total Environ. 409, 3078–3081. https://doi.org/10.1016/j.scitotenv.2011.04.039.
Tian, H., Cheng, K., Wang, Y., Zhao, D., Lu, L., Jia, W., Hao, J., 2012. Temporal and spatial variation characteristics of atmospheric emissions of Cd, Cr, and Pb from coal in China. Atmos. Environ. 50, 157–163. https://doi.org/10.1016/j.atmosenv.2011.12.045.
Tian, H., Liu, K., Zhou, J., Lu, L., Hao, J., Qiu, P., Gao, J., Zhu, C., Wang, K., Hua, S., 2014. Atmospheric emission inventory of hazardous trace elements from China's coal-fired power plants—temporal trends and spatial variation characteristics. Environ. Sci. Technol. 48, 3575–3582. https://doi.org/10.1021/es404730j.
Upadhyay, N., Clements, A., Fraser, M., Herckes, P., 2011. Chemical speciation of PM2.5 and PM10 in South Phoenix, AZ. J. Air Waste Manag. Assoc. 61, 302–310. https://doi.org/10.3155/1047-3289.61.3.302.
Venzac, H., Sellegri, K., Villani, P., Picard, D., Laj, P., 2009. Seasonal variation of aerosol size distributions in the free troposphere and residual layer at the puy de Dôme station, France. Atmos. Chem. Phys. 9, 1465–1478.
Visser, S., Slowik, J., Furger, M., Zotter, P., Bukowiecki, N., Canonaco, F., Flechsig, U., Appel, K., Green, D., Tremper, A., 2015a. Advanced source apportionment of size-resolved trace elements at multiple sites in London during winter. Atmos. Chem. Phys. 15, 11291–11309.
Visser, S., Slowik, J., Furger, M., Zotter, P., Bukowiecki, N., Dressler, R., Flechsig, U., Appel, K., Green, D., Tremper, A., 2015b. Kerb and urban increment of highly time-resolved trace elements in PM 10, PM 2.5 and PM 1.0 winter aerosol in London during ClearfLo 2012. Atmos. Chem. Phys. 15, 2367–2386.
Wang, Q., He, X., Huang, X.H.H., Griffith, S.M., Feng, Y., Zhang, T., Zhang, Q., Wu, D., Yu, J.Z., 2017. Impact of secondary organic aerosol tracers on tracer-based source apportionment of organic carbon and PM2.5: a case study in the Pearl River Delta, China. ACS Earth Space Chem. 1, 562–571. https://doi.org/10.1021/acsearthspacechem.7b00088.
Wang, Q., Qiao, L., Zhou, M., Zhu, S., Griffith, S., Li, L., Yu, J.Z., 2018. Source apportionment of PM2.5 using hourly measurements of elemental tracers and major constituents in an urban environment: investigation of time-resolution influence. J. Geophys. Res. Atmos. 123, 5284–5300. https://doi.org/10.1029/2017JD027877.
Wu, Y.-S., Fang, G.-C., Lee, W.-J., Lee, J.-F., Chang, C.-C., Lee, C.-Z., 2007. A review of atmospheric fine particulate matter and its associated trace metal pollutants in Asian countries during the period 1995–2005. J. Hazard. Mater. 143, 511–515. https://doi.org/10.1016/j.jhazmat.2006.09.066.
Xie, M., Hannigan, M.P., Dutton, S.J., Milford, J.B., Hemann, J.G., Miller, S.L., Schauer, J.J., Peel, J.L., Vedal, S., 2012. Positive matrix factorization of PM2.5: comparison and implications of using different speciation data sets. Environ. Sci. Technol. 46, 11962–11970. https://doi.org/10.1021/es302358g.
Zanobetti, A., Schwartz, J., 2009. The effect of fine and coarse particulate air pollution on mortality: a national analysis. Environ. Health Perspect. 117.
Zhang, L., Wang, S., Wang, L., Wu, Y., Duan, L., Wu, Q., Wang, F., Yang, M., Yang, H., Hao, J., Liu, X., 2015. Updated emission inventories for speciated atmospheric mercury from anthropogenic sources in China. Environ. Sci. Technol. 49, 3185–3194. https://doi.org/10.1021/es504840m.
Zhang, X.-X., Sharratt, B., Liu, L.-Y., Wang, Z.-F., Pan, X.-L., Lei, J.-Q., Wu, S.-X., Huang, S.-Y., Guo, Y.-H., Li, J., 2018. East Asian dust storm in May 2017: observations, modeling, and its influence on the Asia-Pacific region. Atmos. Chem. Phys. 18, 8353–8371.

Zhang, Y.-L., Cao, F., 2015. Fine particulate matter (PM 2.5) in China at a city level. Sci. Rep. 5, 14884.
Zhao, T.L., Gong, S.L., Zhang, X.Y., Jaffe, D.A., 2008. Asian dust storm influence on North American ambient PM levels: observational evidence and controlling factors. Atmos. Chem. Phys. 8, 2717–2728. https://doi.org/10.5194/acp-8-2717-2008.
Zoller, W.H., Gladney, E., Duce, R.A., 1974. Atmospheric concentrations and sources of trace metals at the South Pole. Science 183, 198–200.